VI Congresso Nacional de Mecânica Aplicada e Computacional
Aveiro, 17 a 19 Abril de 2000

PREDICTION OF VISCOELASTIC FLOWS WITH A HIGH-RESOLUTION FINITE-VOLUME METHOD

Manuel A. Alves[1], Fernando T. Pinho[2] e Paulo J. Oliveira[3]

ABSTRACT

This work reports the implementation of a stable high-resolution convective scheme to improve the accuracy and convergence rate of finite-volume predictions of viscoelastic flows. The MINMOD scheme of Harten[1] combines efficiently two second-order differencing schemes (linear-upwind and central differences) in such a way that it completely satisfies the convection boundedness criterion of Gaskell and Lau[2]. The boundedness property of the MINMOD scheme avoids the oscillations in the solution in regions of sharp stress gradients that are usually observed when high-order schemes are used to represent the stress derivatives in the constitutive equation.

To test the accuracy and robustness of the method we selected the popular benchmark flow of a viscoelastic fluid through a 4:1 plane contraction. The constitutive equations selected were those for the Oldroyd-B and upper-convected Maxwell (UCM) fluids. The MINMOD scheme converged in three consecutively refined meshes up to a Deborah number of 5, which is well beyond those attained by other second-order schemes, and most of the calculations encountered in the literature[3]. Using a consistent mesh refinement technique, and applying Richardson's extrapolation, we obtain very accurate results.

1. INTRODUCTION

The design of extrusion dies for polymer melt processing is a relevant industrial application of software aimed at predicting viscoelastic flows. Contractions and expansions occur naturally in such devices, but numerical methods can suffer from convergence problems whenever there are very sudden geometrical variations coupled with high levels of elasticity[4]. The sudden contraction suffers from such problems, which allied to its

[1] Faculdade de Engenharia da Univ. do Porto, Dep. Eng. Química, CEFT, 4050-123 Porto (mmalves@fe.up.pt).
[2] Faculdade de Engenharia da Univ. do Porto, Dep. Eng. Mecânica, CEFT, 4050-123 Porto (fpinho@fe.up.pt).
[3] Universidade da Beira Interior, Dep. Eng. Electromecânica, 6200 Covilhã (pjpo@ubi.pt).

geometrical simplicity made it an extensively used tool for benchmarking the development of robust calculation methods[5], especially the 4:1 contraction ratio version.

Finite-volume methods (FVM) are advantageous relative to finite-element methods (FEM) due to their inherent economy of computational resources[6], but until the late eighties the development of numerical methods for viscoelastic flow predictions has been mostly based on the later technique. Over the last five years major progress has taken place on the development of FVM for viscoelastic flow predictions: initially based on orthogonal and staggered meshes[7,8], the method has evolved rapidly to handle block-structured[9] and non-structured meshes[6], and simultaneously there has been some limited progress in accuracy with the evolution from first-order to second-order discretisation schemes for representing the convective terms in the constitutive equations[10]. These workers found that the limited success of high-order schemes in terms of convergence was attributed to the lack of delimiters, and so the issue can be solved by the adoption of the so-called high-resolution schemes (HRS)[11]. Basically, the HRS combine high-order schemes with the enforcement of adequate boundedness criteria everywhere in the flow field and especially in regions of high stress gradients.

In this work an HRS is incorporated for the first time into a FVM based code operating with collocated meshes and tested in the 4:1 sudden contraction benchmark viscoelastic flow. Improvements in the accuracy and the extent of Deborah numbers over which there is a consistent accurate prediction of flow characteristics are some of the important effects investigated here.

The next section describes the governing equations and is followed by the numerical method and geometry definition. The results are presented and discussed afterwards and the paper ends with a brief summary of the main conclusions.

2. GOVERNING EQUATIONS

The basic equations to be solved are those for two or three-dimensional, incompressible and isothermal laminar flow of an Oldroyd-B fluid. In Cartesian tensor notation they are the continuity equation

$$\frac{\partial u_i}{\partial x_i} = 0 \tag{1}$$

the equation for conservation of linear momentum

$$\frac{\partial r u_i}{\partial t} + \frac{\partial r u_j u_i}{\partial x_j} - \frac{\partial}{\partial x_j}\left(h \frac{\partial u_i}{\partial x_j} \right) = -\frac{\partial p}{\partial x_i} + \frac{\partial t_{ij}}{\partial x_j} - \frac{\partial}{\partial x_j}\left(h \frac{\partial u_i}{\partial x_j} \right) \tag{2}$$

and the constitutive equation[12]

$$t_{ij} = h_s \left(\frac{\partial u_i}{\partial x_j} + \frac{\partial u_j}{\partial x_i} - \frac{2}{3}\frac{\partial u_k}{\partial x_k} d_{ij} \right) + t_{ij_e} \tag{3.1}$$

$$t_{ij_e} + l\left(\frac{\partial t_{ij_e}}{\partial t} + \frac{\partial u_k t_{ij_e}}{\partial x_k} \right) = l\left(t_{ik_e}\frac{\partial u_j}{\partial x_k} + t_{jk_e}\frac{\partial u_i}{\partial x_k} \right) + h_p \left(\frac{\partial u_i}{\partial x_j} + \frac{\partial u_j}{\partial x_i} - \frac{2}{3}\frac{\partial u_k}{\partial x_k} d_{ij} \right). \tag{3.2}$$

where r is the density of the fluid, u_i is the velocity component along the Cartesian co-ordinate x_i, p is the pressure, l is the relaxation time, d_{ij} is the Kronecker delta, h_s is the shear viscosity of the Newtonian solvent and h_p is the contribution of the polymer molecule to the total shear viscosity $h = h_s + h_p$. The Newtonian model is obtained using $l = 0$ and the

upper-convected Maxwell model (UCM) is recovered in this formulation by setting $h_s = 0$. t_{ije} represents the contribution of the polymer molecules to the total stress tensor.

The terms on the l.h.s. of Eqs (2) and (3.2) are dealt with implicitly, while those on the r.h.s. go into the source term of the matrix equations resulting from the discretisation procedure. The addition and subtraction of the normal diffusion term in Eq. (2) is for numerical convenience gained from experience with Newtonian computations. It brings the final equations into the standard convection/diffusion form and the calculation method remains completely general regardless of the adopted constitutive equation The diffusion term on the r.h.s. of Eq. (2) will lag for a time step in the time advancement solution method, but this practice does not affect the final steady state solution[9].

Although the Oldroyd-B and the UCM are two of the simplest models to represent viscoelasticity, they are the most challenging from the numerical point of view because, of all constitutive models, they tend to develop the highest stress growth-rate near singularities.

3. FINITE-VOLUME NUMERICAL METHOD

The equations of the previous section are transformed into a general nonorthogonal co-ordinate system for easy application of the FVM to a collocated mesh arrangement. The equations are then integrated over the set of control volumes (cells) and discretised. The dependent variables remain the Cartesian velocity and stress components and the pressure, all stored at the centre of the cells. To avoid stress-velocity decoupling, a special procedure explained in detail in the previous works[9,13] is adopted for the calculation of the stress divergent term in the momentum equation. The novelty of the method in this work is the MINMOD high-resolution scheme used to interpolate the cell-face stresses originating in the convective terms of the constitutive equation, therefore only this issue will be addressed in detail below.

The discretised form of the constitutive equation is casted in the usual form, at a general cell P of volume V_P,

$$a_P t_{ij_e,P} - \sum_F a_F t_{ij_e,F} = S_{t_{ij_e}} + \frac{l_P V_P}{dt} t^0_{ij_e,P}. \qquad (4)$$

As there is no diffusion of stress in the constitutive equation, the coefficients a_F are composed only by convective contributions. In the present procedure the MINMOD[1] HRS is used together with the deferred correction approach[14]. The HRS denote the class of composite high-order schemes that are bounded and have relatively low numerical diffusion, and in this work its implementation is made according to the normalised variable and space formulation (NVSF)[11]. In the NVSF the convected stress component t_{ij} (or any other convected variable, f) and the general curvilinear co-ordinate x are normalised as

$$\hat{t}_{ij} = \frac{t_{ij} - t_{ij,U}}{t_{ij,D} - t_{ij,U}}; \quad \hat{x} = \frac{x - x_U}{x_D - x_U} \qquad (5)$$

where the subscripts U and D refer to the upstream and downstream cells to cell P which is, itself, located immediately upstream of cell face f under consideration (see Fig. 1.*a*).

To satisfy the convection boundedness criterion (CBC) of Gaskell and Lau[2] the functional relationship of an interpolation scheme applied to a cell-face f, $\hat{t}_{ij,f} = J(\hat{t}_{ij,P})$, must be bounded, as represented in Fig. 1 (*b*) by the triangular area together with the line with slope 1 (representing the upwind scheme). The various straight lines in this figure are for the UDS (upwind), the LUDS (linear upwind) and the CDS (central differencing) schemes.

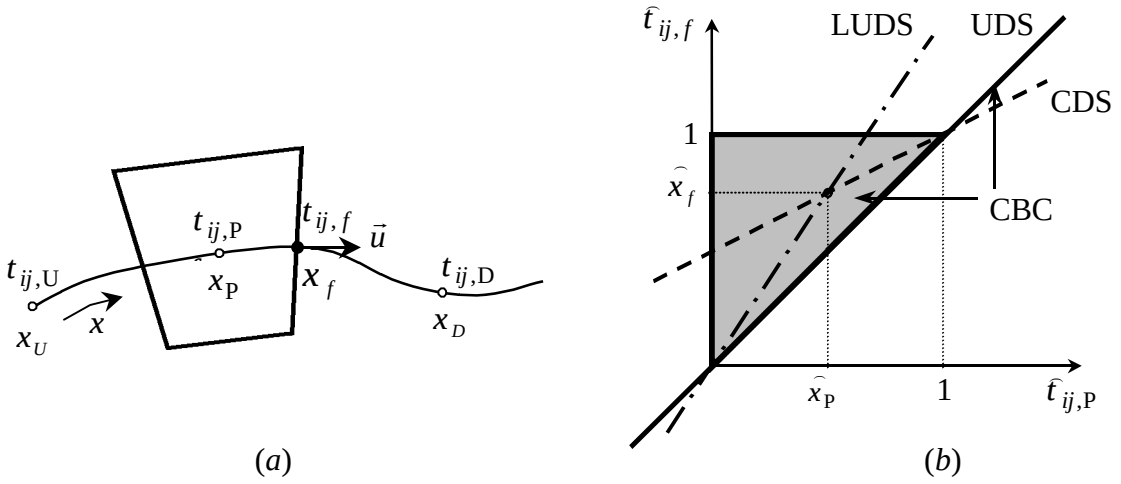

(*a*) (*b*)

Fig. 1- (*a*) Definition of local variables and co-ordinate system. (*b*) Normalised variable diagram (NVD) for different interpolating schemes and showing the CBC.

Fig. 1 (*b*) shows that the lines representing the second-order LUDS and CDS schemes do not completely satisfy the CBC criterion in the whole range. It is, however, possible to combine them into a composite HRS, which satisfies the CBC criterion, and take the form

$$\hat{t}_{ij,f} = \begin{cases} \dfrac{\hat{x}_f}{\hat{x}_P}\hat{t}_{ij,P} & 0 < \hat{t}_{ij,P} < \hat{x}_P \qquad \text{(LUDS)} \\ \dfrac{1-\hat{x}_f}{1-\hat{x}_P}\hat{t}_{ij,P} + \dfrac{\hat{x}_f - \hat{x}_P}{1-\hat{x}_P} & \hat{x}_P \le \hat{t}_{ij,P} < 1 \qquad \text{(CDS)} \\ \hat{t}_{ij,P} & \textit{elsewhere} \qquad \text{(UDS)} \end{cases} \tag{6}$$

Applying the MINMOD scheme to the convective fluxes in the stress equation, and after a bit of algebra, these become

$$\frac{l}{r}F_f \hat{t}_{ij,f} = \frac{l}{r}F_f t_{ij,C} + \frac{l}{r}F_f \left[a\left(t_{ij,D} - t_{ij,U}\right) + (b-1)\left(t_{ij,C} - t_{ij,U}\right)\right]_f . \tag{7}$$

With the fluxes written under this form, we recognise the first term on the r.h.s. of Eq. (7) as being the flux for the upwind scheme while the term in square brackets arises from the HRS. In spite of its disadvantages regarding accuracy, the UDS scheme possesses an inherent stability advantage, which can be used to profit in the deferred correction approach[14]. With the deferred correction, a high-order or high-resolution scheme can be easily implemented into a numerical procedure designed for the upwind scheme. The coefficients of the discretised stress equations are kept as those for the UDS, and contain the first part of the flux (7), while the remaining part of (7) is inserted into the source term of Eq. (4), and is thus treated explicitly in the context of the time advancement. While this explicit addition of some of the convective flux terms may lead to a relative slowdown of the iterative-like procedure, the simplicity of implementation of the deferred correction approach together with the important memory-saving fact that the coefficients a_F and a_P are then the same for all the six stress equations, make this approach very appealing and it is thus adopted here.

4. FLOW GEOMETRY AND COMPUTATIONAL MESH

In this work we used the popular benchmark flow through a 4:1 planar contraction, as sketched in Fig. 2. The figure defines the co-ordinate system, some of the relevant

nomenclature and shows the five structured blocks used to generate the three consecutively refined meshes.

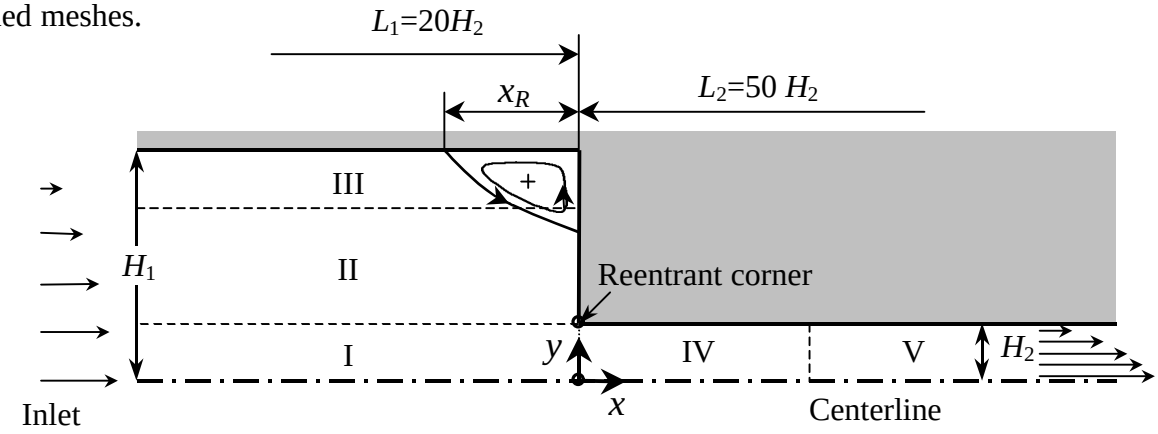

Fig. 2- Schematic representation of the 4:1 planar contraction.

The computational meshes used are orthogonal, but non-uniform, with increased concentration of cells near the reentrant corner and the upstream wall where the stress gradients are expected to be higher. In previous work[9,13] it was found that a computational domain extending from x=-20H_2 to x=50H_2 is appropriate for the present problem.

The cell size inside each of the five blocks used in a given mesh varied in geometrical progression at a constant ratio. In order to guarantee a smooth cell-size variation inside and in-between the patched sub-blocks the contraction factors were chosen to be near unity for the finest meshes. During mesh refinement the number of cells along each direction was doubled, and the corresponding expansion/contraction ratios inside each sub-block were root-squared. This procedure ensured a consistent mesh refinement, with the grid spacing being approximately halved between consecutive meshes, thus enabling error estimation using Richardson's extrapolation to the limit[15]. In Fig. 3 a zoomed view of the finest mesh is shown, where the minimum non-dimensional cell size is only 0.01 in both the x- and y-directions near the re entrant corner. As we shall show this level of refinement coupled with a high-resolution scheme allowed us to obtain very accurate solutions, especially for low Deborah values.

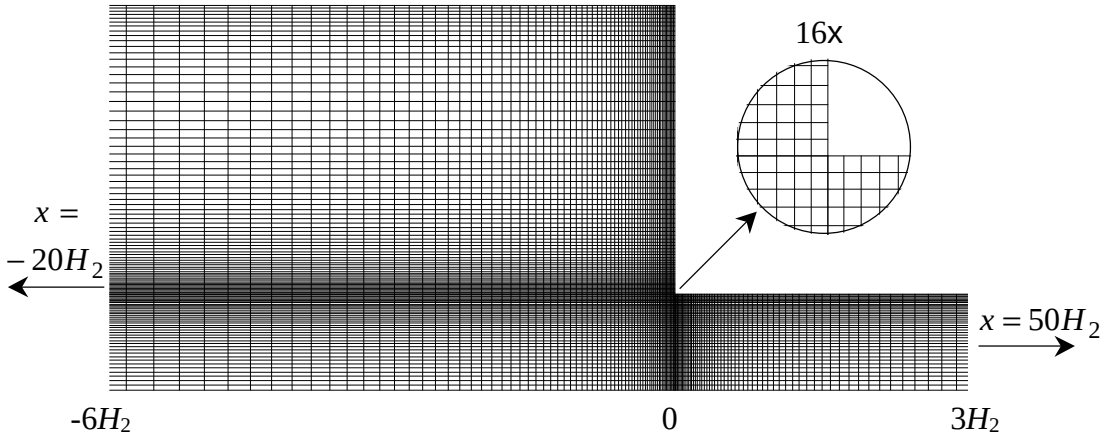

Fig. 3- Zoomed view of the finest mesh used in the calculations (mesh 3).

The important characteristic parameters for this flow are the Reynolds number, and the Deborah number, the latter being a measure of the elasticity level of the flow. Both are defined on the basis of downstream quantities:

$$Re = \frac{rU_2H_2}{h}\ ,\ De = \frac{lU_2}{H_2}\ . \qquad (8)$$

For the Oldroyd-B model there is a third relevant parameter, namely the relative solvent viscosity with respect to the total viscosity, $b = h_s / h$, but throughout this work it was taken as b=1/9, for which substantial results are available for comparison[3].

5. RESULTS

Our finite-volume code was used in the simulation of the viscoelastic contraction flow in order to investigate the effects of mesh refinement and differencing scheme in the flow patterns. The effect of the elasticity level of the flow was investigated by varying the Deborah number at creeping flow conditions, and the effect of inertia was studied for Newtonian, and Oldroyd-B model at *De*=2.

5.1 Influence of mesh fineness and differencing scheme in the flow patterns

In order to accurately simulate the viscoelastic contraction flow, very refined meshes are required in conjunction with high-order or high-resolution schemes, as demonstrated in our previous work[16]. In that work it was found that the MINMOD scheme has approximately second-order accuracy, and the UDS scheme is only first-order, as already expected. It was also shown that in order to apply Richardson's extrapolation a fourth mesh (with 57 032 cells!) was needed for the UDS scheme. This very refined mesh (to our knowledge is the finest mesh used so far in this problem) needs large computational resources and the large computational times involved make this research quite laborious.

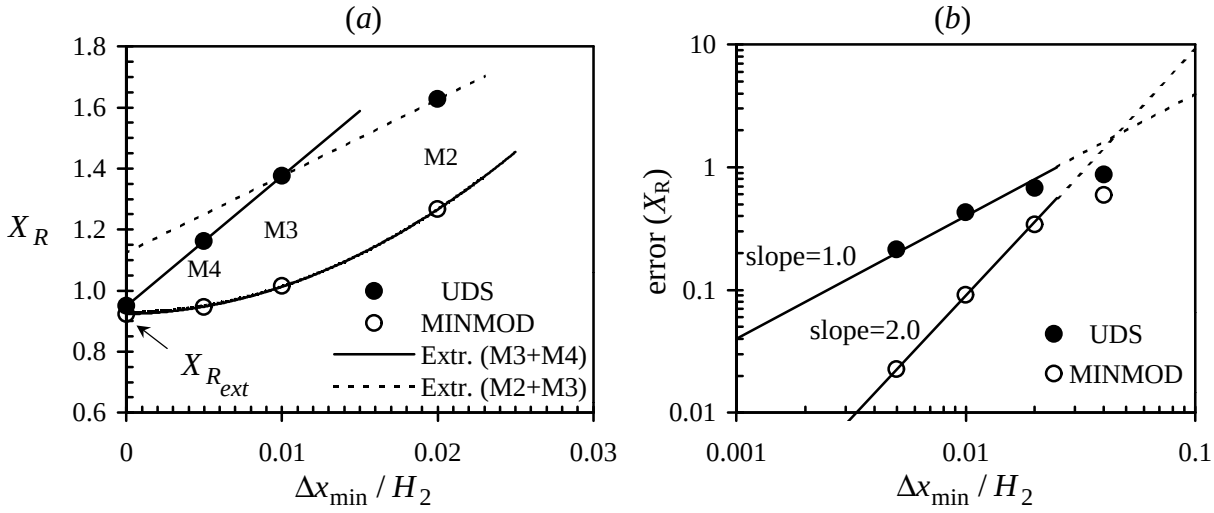

Fig. 4- (*a*) Vortex size dimension and (*b*) absolute error in X_R as a function of the minimum cell-size, for the UDS and MINMOD schemes with an UCM fluid. Data from [16].

For the MINMOD scheme it was found that the 3 meshes used in this work are sufficient, and so we restrict this work to this scheme. In Fig. 4 we reproduce the results previously obtained[16] for the UCM model at *Re*=0.01 and *De*=3 to illustrate the above conclusions. The flow parameter used to assess the true order of accuracy was the dimensionless vortex size dimension, $X_R=x_R/H_2$ (see Fig. 2).

In Fig. 5 the effect of mesh refinement is shown for the dimensionless first-normal stress difference, $N_1/T_w=(t_{xx}-t_{yy})/(3hU_2/H_2)$. The results presented were obtained along the line y/H_2=0.98, for the Newtonian and UCM model at *De*=3[16]. The Reynolds number in both cases is 0.01, which is representative of creeping flow conditions. The UCM model develops large stresses near the reentrant corner and along the downstream channel wall, which require

the use of very fine meshes coupled with high-resolution schemes. The convergence with mesh refinement is also evident.

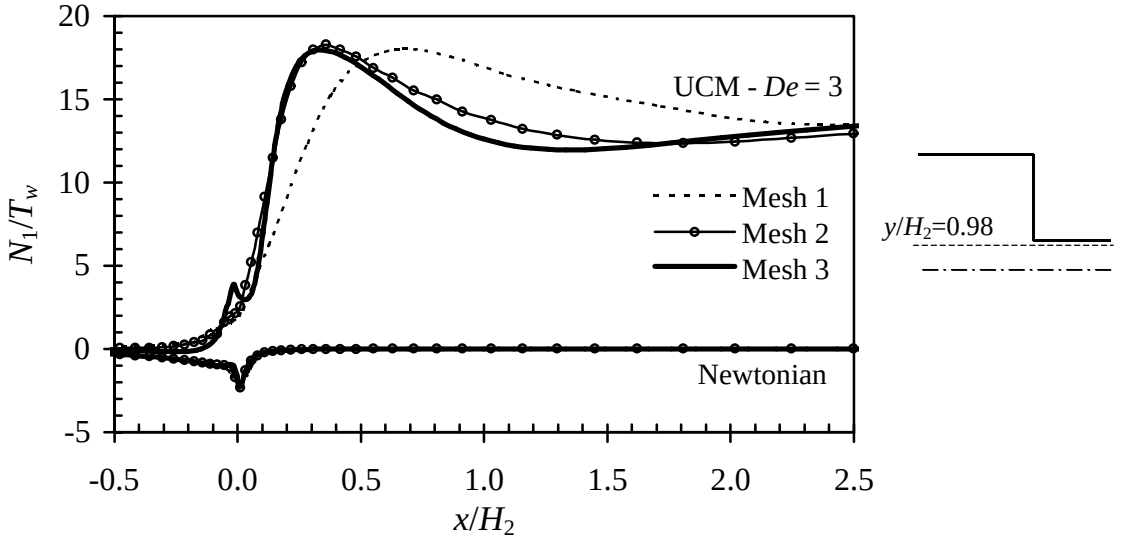

Fig. 5- First-normal stress difference along the line y/H_2=0.98 at creeping flow conditions, for the Newtonian and UCM models, with the MINMOD scheme.

5.2 Influence of elasticity in the flow patterns at creeping flow conditions

The influence of elasticity was studied for both the UCM and Oldroyd-B fluids under creeping flow conditions.

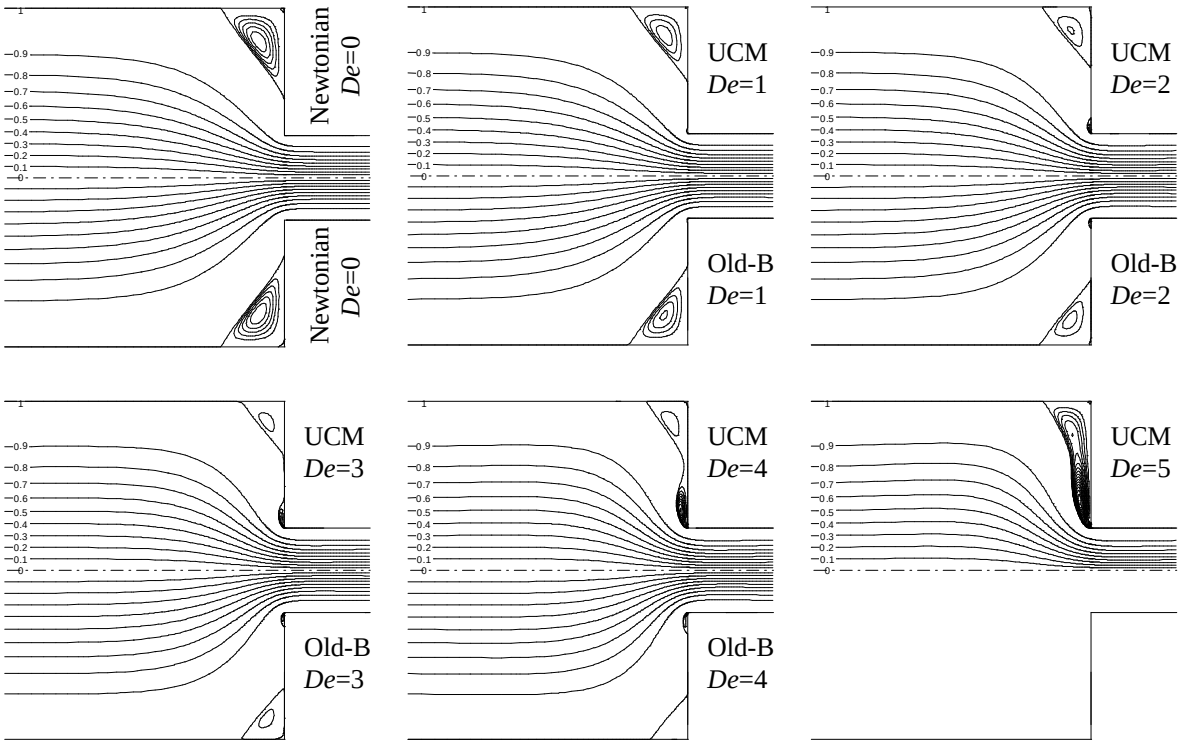

Fig. 6- Predicted streamlines obtained in the fine mesh with the MINMOD scheme for the UCM (upper half of the channels) and Oldroyd-B models, at creeping flow conditions. The streamlines in the recirculations are equally spaced with $d_\Psi = 2 \times 10^{-4}$.

Figure 6 presents the streamlines obtained in mesh 3 with the MINMOD scheme for the UCM and Oldroyd-B models, varying the Deborah number up to 5. Convergence was obtained for higher Deborah numbers with the coarser meshes, but these results suffer from lack of accuracy, as can be assessed from Fig. 7, and were not considered here. For the Oldroyd-B model convergence failed above *De*=4, for the finest mesh 3, which was rather unexpected, since this model is expected to be more stable than the UCM. Further research will be conducted soon in order to stabilize the Oldroyd-B model. It should however be emphasized that our limiting Deborah number values are above those usually reported in literature[3], coupled with the fact that our meshes are much finer. Furthermore, we use a HRS which greatly enhances the accuracy of the results, as can be assessed from Fig. 7. It is worth mention that although the contraction flow was one of the first benchmarks used in viscoelastic flows, now, more than 20 years later, there is still no agreement over simple quantitative parameters such as the vortex length and strength. To ilustrate this fact, in Figure 8 we reproduce our results in conjunction with some of the results obtained from the literature. The comparison is made for the dimensionless primary vortex length and for the maximum recirculation intensity which was normalised by the flowrate, $\Psi_{max}=(y_{max}/U_2H_2)-1$. The literature results are in relative agreement with the results obtained in our coarsest mesh, however these are very different from the more correct results obtained using more refined meshes and applying Richardson's extrapolation to the limit.

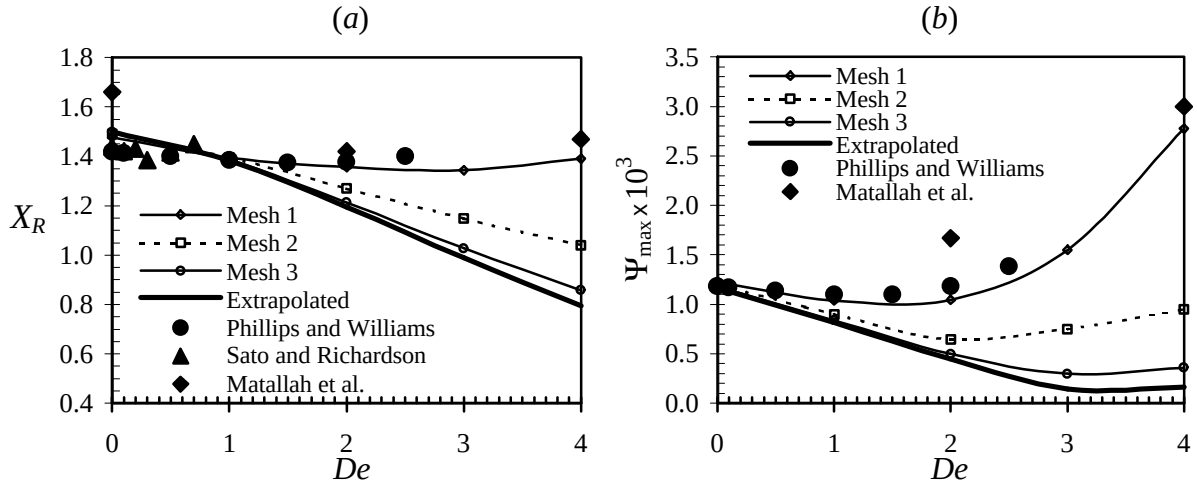

Fig. 7- (*a*) Vortex dimension and (*b*) maximum recirculation intensity as a function of Deborah number for Oldroyd-B model at *Re*=0. Comparison with literature results.

With both the UCM and Oldroyd-B fluids we see the development of a lip vortex at Deborah numbers less than 1, and its growth with elasticity. With the UCM fluid the lip vortex grows so much that it grows towards the salient corner vortex. Its growth is so strong that eventually it overcomes the salient corner vortex as a result of the high stresses that develop in the vicinity of the reentrant corner. The merge process is absent for the Oldroyd-B fluid since the developed stresses are not so intense. It may also be that it would occur at higher *De*.

5.3 Influence of inertia in the flow patterns for the Newtonian and Oldroyd-B model at *De*=2

The above calculations were performed for creeping flow conditions. However, it is known that the inclusion of inertia leads to a reduction in vortex size and strength[3]. In Fig. 8 we present the streamlines obtained varying the Reynolds number for the Newtonian and Oldroyd-B model at *De*=2. With an increasing Reynolds number there is a significant

decrease in the primary vortex size and intensity for both the Newtonian and Oldroyd-B model as inertia pushes the secondary flow towards the contraction wall. The lip-vortex that appears for the Oldroyd-B fluid is only slightly affected by inertia. Finally, in Fig. 9 we represent the values of X_R and Ψ calculated using Richardson's extrapolation, as a function of the Reynolds number. For the Oldroyd-B model convergence failed above *Re*=2, and for the Newtonian case we decided not to pursue the calculations any further.

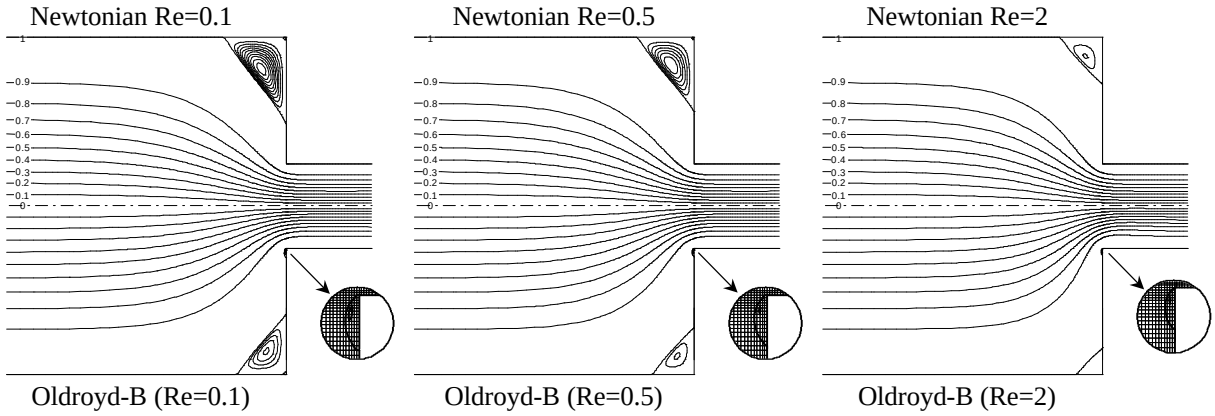

Fig. 8- Predicted streamlines obtained in the fine mesh with the MINMOD scheme for the Newtonian (upper half of the channels) and Oldroyd-B model at *De*=2. The streamlines in the recirculations are equally spaced with $d_\Psi=10^{-4}$. A zoomed view of the lip vortex is shown.

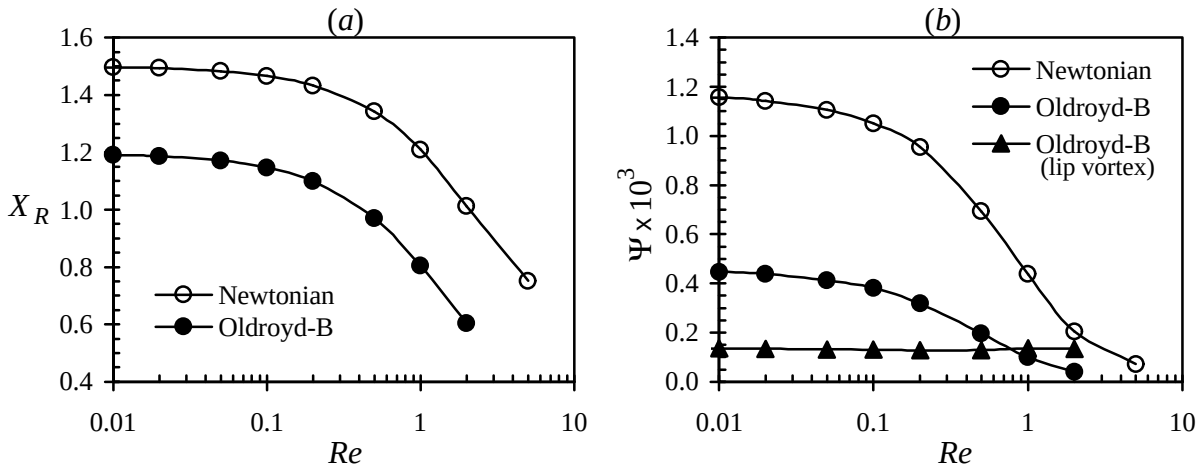

Fig. 9- (*a*) Dimensionless primary vortex length and (*b*) recirculation strength as a function of the Reynolds number, for the Newtonian and Oldroyd-B fluid at *De*=2.

6. CONCLUSIONS

A high-resolution scheme was successfully implemented into a finite-volume based code for predictions of viscoelastic flows and tested in the 4:1 planar sudden contraction benchmark flow. The HRS was used to represent the convective terms of the constitutive equations, here the UCM and Oldroyd-B fluids. The calculations were seen to be second order accurate and convergence was attained at higher Deborah numbers (*De*=5 with UCM) than previously when we used the second order upwind scheme (*De*=1 with UCM).

The work shows the main differences between the behaviour of UCM and Oldroyd-B fluids and also quantifies the effect of Reynolds number in reducing the size and strength of the salient and lip vortex of Newtonian and Oldroyd-B fluids.

ACKNOWLEDGEMENTS

M. A. Alves is a member of staff at Departamento de Engenharia Química, FEUP, and wishes to thank his colleagues for a temporary leave of absence.

REFERENCES

[1] Harten, A., High resolution schemes for hyperbolic conservation laws, *J. Comput. Phys.* **49** 357-393 (1983).

[2] Gaskell, P.H. and A.K.C. Lau, Curvature compensated convective transport: SMART, a new boundedness preserving transport algorithm, *Int. J. Numer. Meth. Fluids* **8** 617-641 (1988).

[3] Phillips, T. N. and A. J. Williams, Viscoelastic flow through a planar contraction using a semi-Lagrangian finite volume method, *J. Non-Newt. Fluid Mech.* **87** 215-246 (1999).

[4] Crochet, M. J., A. R. Davies and K. Walters, "Numerical simulation of non-Newtonian flow", Elsevier Rheology Series, Vol. 1, 1984.

[5] Brown, R. A. and G. H. McKinley, Report on the VIIIth International Workshop on Numerical Methods in Viscoelastic Flows, *J. Non-Newt. Fluid Mech.* **52** 407-413 (1994).

[6] Huang, X., N. Phan-Thien and R.I. Tanner, Viscoelastic flow between eccentring rotating cilynders: unstructured control volume method, *J. Non- Newt. Fluid Mech.* **64** 71-92 (1996).

[7] Yoo, J.Y.and Y. Na, A numerical study of the planar contraction flow of viscoelastic fluids using the SIMPLER algorithm, *J. Non- Newt. Fluid Mech.* **39** 89-106 (1991).

[8] Sasmal, G.P., A finite volume approach for calculation of viscoelastic flow through an abrupt axisymetric contraction, *J. Non- Newt. Fluid Mech.* **56** 14-47 (1995).

[9] Oliveira, P.J., F.T. Pinho and G.A. Pinto, Numerical simulation of non-linear elastic flows with a general collocated finite-volume method, *J. Non-Newt. Fluid Mech.* **79** 1-43 (1998).

[10] Oliveira, P.J. and F.T. Pinho, Plane contraction flows of upper convected Maxwell and Phan-Thien—Tanner fluids as predicted by a finite-volume method, *J. Non-Newt. Fluid Mech.* **88** 63-88 (1999).

[11] Darwish, M.S. and F. Moukalled, Normalized variable and space formulation methodology for high-resolution schemes, *Numer. Heat Transfer*, Part B **26** 79-96 (1994).

[12] Bird, R.B., R.C. Armstrong and O. Hassager, "Dinamics of Polimeric Liquids", 2nd ed., Vol. 1: Fluid Mechanics, Wiley, New York, 1987.

[13] Oliveira, P.J. and F.T. Pinho, Numerical procedure for the computation of fluid flows with arbitrary strss-strain relationships, *Num. Heat Transfer*, Part B **35** 295-315 (1999).

[14] Khosla, P.K. and S. G. Rubin, A diagonally dominant second-order accurate implicit scheme, *Computers and Fluids* **2** 207-209 (1974).

[15] Ferziger, J. H. and M. Peric, Further discussion of numerical errors, *Int. J. Num. Meth. Fluids* **23** 1263-1274 (1996)

[16] Alves, M. A., F. T. Pinho and P. J. Oliveira, Effect of a high-resolution differencing scheme on finite-volume predictions of viscoelastic flows. Submitted to *J. Non-Newt. Fluid Mech.*

[17] Matallah, H., P. Towsend and M. F. Webster, Recovery ans stress-splitting schemes for viscoelastic flows, *J. Non-Newt. Fluid Mech.* **75** 139-166 (1998).

[18] Sato, T. and S. M. Richardson, Explicit numerical simulation of time-dependent viscoelastic flow problems by a finite element/finite volume method, *J. Non-Newt. Fluid Mech.* **51** 249-275 (1994).